

PT-PINNs: A Parametric Engineering Turbulence Solver based on Physics-Informed Neural Networks

Liang Jiang,¹ Yuzhou Cheng,² Kun Luo,^{1,*} and Jianren Fan¹

¹State Key Laboratory of Clean Energy Utilization, Zhejiang University, Hangzhou, China

²Shanghai Institute for Advanced Study of Zhejiang University, Shanghai, China

Physics-informed neural networks (PINNs) demonstrate promising potential in parameterized engineering turbulence optimization problems but face challenges, such as high data requirements and low computational accuracy when applied to engineering turbulence problems. This study proposes a framework that enhances the ability of PINNs to solve parametric turbulence problems without training datasets from experiments or CFD-Parametric Turbulence PINNs (PT-PINNs)). Two key methods are introduced to improve the accuracy and robustness of this framework. The first is a soft constraint method for turbulent viscosity calculation. The second is a pre-training method based on the conservation of flow rate in the flow field. The effectiveness of PT-PINNs is validated using a three-dimensional backward-facing step (BFS) turbulence problem with two varying parameters ($Re_h = 3000-200000$, $ER = 1.1-1.5$). PT-PINNs produce predictions that closely match experimental data and computational fluid dynamics (CFD) results across various conditions. Moreover, PT-PINNs offer a computational efficiency advantage over traditional CFD methods. The total time required to construct the parametric BFS turbulence model is 39 hours, one-sixteenth of the time required by traditional numerical methods. The inference time for a single-condition prediction is just 40 seconds—only 0.5% of a single CFD computation. These findings highlight the potential of PT-PINNs for future applications in engineering turbulence optimization problems.

Solving turbulent flow fields plays a critical role in engineering applications such as combustion chamber design [1], aerodynamic optimization of vehicles [2], and thermal management of motors and chips [3]. Over the past decades, various numerical methods, including the finite difference method (FDM) [4], finite volume method (FVM) [5], finite element method (FEM) [6], spectral method [7], and Lattice Boltzmann method (LBM) [8], have been developed and applied to solve turbulent flow fields. These methods are typically based on discretization techniques and predict flow behavior by numerically solving the Navier-Stokes equations. However, it is often necessary to parameterize the turbulent flow field in practical engineering design. For problems with varying geometries and boundary conditions, these methods often require multiple simulations. In such cases, even with the use of methods such as large eddy simulation (LES) [9] or Reynolds-averaged navier-stokes simulation (RANS) [10], these numerical methods still consume significant time and energy to solve the flow fields under multiple operating conditions [2]. At the same time, the vast amounts of data generated from multiple simulations often hinder storage and retrieval, increasing the difficulty of building intelligent digital twin systems for modern design, equipment operation, and maintenance.

In recent years, driven by advancements in artificial intelligence, data-driven methods for parameterized flow field solutions have been developed [11–13]. These methods rely on existing experimental or computational fluid

dynamics (CFD) data, leveraging machine learning techniques to train neural networks that take spatial coordinates, geometry, and operating parameters as inputs and output flow field variables. The resulting machine learning models are compact, easily storable, and enable fast inference of flow fields under varying parameters. Operator learning methods such as DeepONet [14] and Fourier Neural Operators (FNO) [15] have recently improved the generalization capabilities of these models through network architecture optimization. However, these models still require extensive datasets for training, and their predictive capabilities degrade significantly when the parameter range is insufficiently represented in the dataset or when the training data lacks accuracy. In many engineering applications, acquiring sufficient high-quality data remains costly and challenging.

Data-driven machine learning surrogate models for flow fields are inherently limited in generalization accuracy and physical interpretability. As a result, physics-driven machine learning methods have recently emerged as a promising paradigm. Raissi et al. [16] introduced the Physics-Informed Neural Networks (PINNs) method for solving partial differential equations (PDEs). Since neural networks are inherently differentiable, automatic differentiation [17] can be used to compute PDE residuals across the entire input space. By incorporating the governing PDEs as loss functions in the neural network training process, functional solutions to PDEs under specific initial and boundary conditions can be obtained. They successfully applied PINNs to solve the cylinder flow problem, achieving highly accurate predictions of flow fields with minimal data requirements [16]. Jin et al.

* Email to: zjulk@zju.edu.cn

[18] applied PINNs to solve two-dimensional (2D) laminar flow around airfoil geometries, demonstrating good agreement with CFD results and showcasing the potential of PINNs for parameterized flow field solutions. Jin et al. [19] proposed a PINNs-based incompressible flow solver, NSFnet, which achieved promising results for turbulent channel flows at $Re_\tau = 1000$.

Despite the potential of PINNs in computational fluid dynamics, their application to turbulent flow problems remains challenging due to the inherent complexity of turbulence. For instance, Pioch et al. [20] demonstrated that PINNs failed to accurately predict 2D backward-facing step (BFS) turbulent flows ($Re=5100$) using $k-\epsilon$ and $k-\omega$ models unless supplemented with direct numerical simulation (DNS) data. Even with partial internal data assimilation, significant deviations persisted in flow field predictions. Yadav et al. [21] applied PINNs to solve 2D turbulent flame, and found that the model could not predict the velocity fields correctly when only the sparse training data of the temperature field was applied. Many other existing studies also reveal critical limitations when applying PINNs to solve turbulence problems without auxiliary data [22, 23].

Recent attempts to address these limitations have yielded mixed outcomes. Cao et al. [24] attempted to use PINNs for the parametrization design of 2D duct flow deflectors ($Re=1 \times 10^5$) and achieved good agreement with CFD results in zero-equation turbulence modeling. However, the method was limited to simplified 2D problems. Meanwhile, Gafoor et al. [25] observed persistent discrepancies between PINNs predictions and experimental data in wind turbine wake studies using $k-\epsilon$ models. To enhance PINNs' capability for multiscale turbulence, advanced architectures such as Time-stepping-oriented Neural Networks (TSOINN) [26, 27], domain decomposition [28], and operator network-based approaches [29] have emerged. However, these methods incur substantial computational costs and lack validation for three-dimensional turbulent flows. Overall, PINNs for solving parameterized engineering flows remain in a preliminary stage, typically limited to laminar flows [30–32] or 2D turbulent flow [24]. Accurately solving three-dimensional high Reynolds number engineering turbulence using two-equation turbulence models with wall functions remains challenging without the assistance of internal flow field data for training.

In this work, we proposed a parameterized turbulent flow field prediction framework based on PINNs. This framework effectively enhances the predictive capability of PINNs for parameterized steady-state turbulent flow field prediction. We applied two training methods within this framework. The first is a soft constraint calculation method for turbulent viscosity, which takes turbulent viscosity as the output of the neural network and transforms the algebraic calculation formula of turbulent viscosity in the two-equation turbulence model into the loss function for turbulent viscosity. The second is a pre-training method based on the conservation of flow rate

in the flow field. We validated the framework's effectiveness through a parameterized turbulent backward-facing step flow problem with $Re_h \in [3000, 200,000]$, incorporating two variable parameters: the step expansion ratio (ER) and fluid viscosity ν . The parametric PINNs model was trained solely using the PDEs of $k-\omega$ turbulence model and boundary conditions. By comparing the predictions of PINNs with CFD results and experimental results from Nadge et al. [33] across different geometric shapes and Reynolds numbers, we demonstrated the framework's reliability. Furthermore, we explored the effects of the two key training methods in this framework. By contrasting the parameterized $k-\omega$ turbulence model for backward-facing step flows under different weight balancing of PDEs and boundary conditions, both with and without these methods, we confirmed their role in enhancing PINNs' ability to balance the losses of multiple complex partial differential equations in turbulence modeling and to avoid convergence to local optima.

RESULTS

Framework Overview

A parametric, steady-state turbulent flow field prediction framework based on PINNs is developed in this study. The process for solving a specific turbulent flow field prediction problem using this framework is illustrated in Fig. 1. PT-PINNs directly employ neural networks to solve parameterized, high-dimensional turbulence problems by feeding both spatial parameters and parameters related to geometric shapes, operating conditions, and fluid properties as inputs into the network. It requires only a single model training session to solve parameterized turbulence problems with multiple variable parameters.

We introduced a pre-training method based on flow field initialization to this framework. The loss function during the pre-training phase consists of parameterized boundary conditions, integral interface constraints, and specified interior numerical constraints based on flow field flux conservation. The number of iterations in the pre-training phase is 1/20th of the total training steps. Upon completion of the pre-training, we employed a transfer learning approach to use the pre-trained network as the initial network for the formal training, thereby accelerating the overall convergence and enhancing training stability. The flowchart of the overall framework is shown in Fig. 1b. In addition to flow field variables such as velocity, pressure, and turbulent kinetic energy, we explicitly defined turbulent viscosity as one of the neural network outputs, although turbulent viscosity can be algebraically computed by two-equation or zero-equation turbulence models. We transformed the algebraic expressions into loss functions to constrain turbulent viscosity as shown in Fig. 1c. This constraint ensures that its effect is nearly equivalent to algebraic computations when

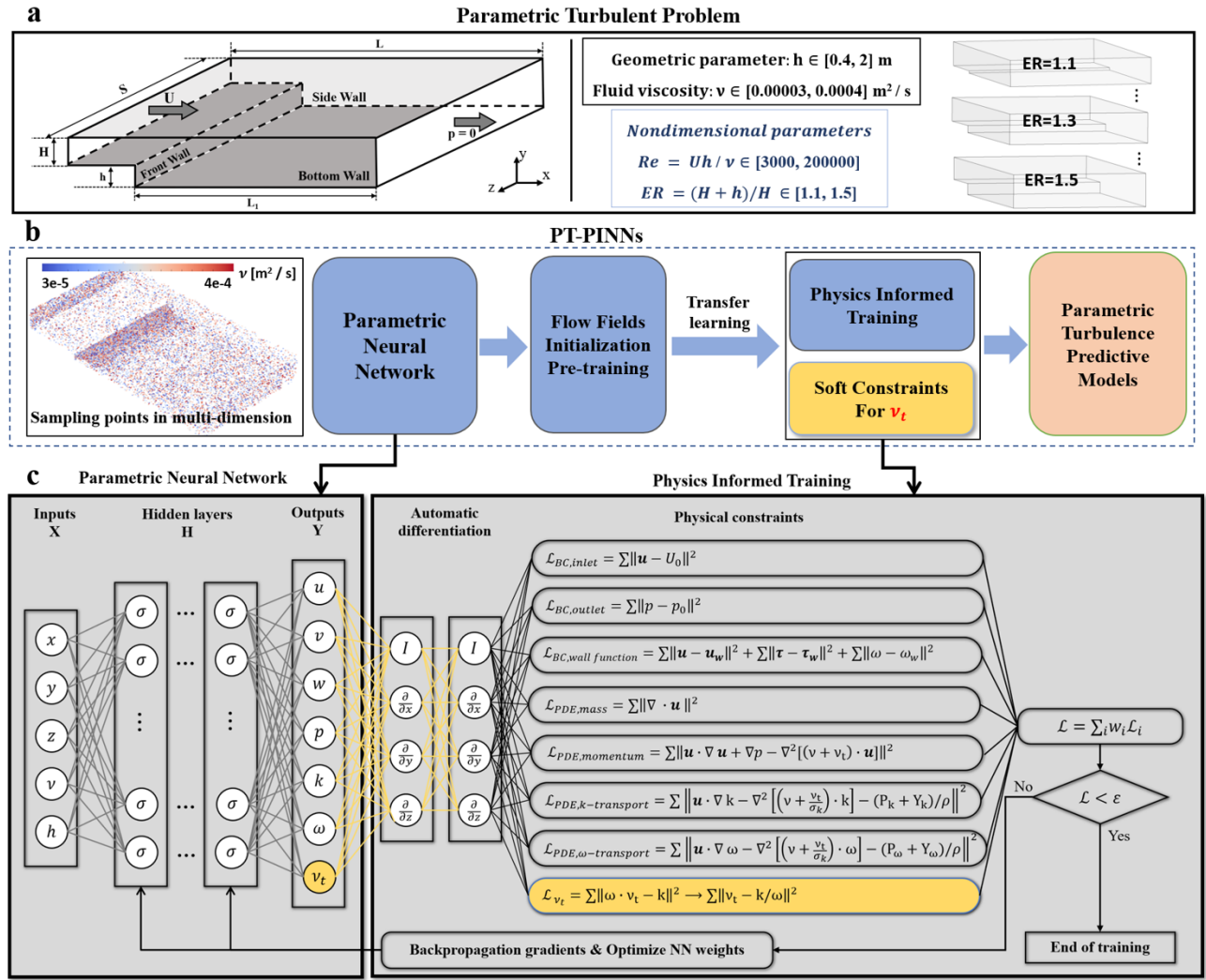


FIG. 1. **The framework of the PT-PINNs.** **a.** The configuration of the parametric 3D turbulent BFS problem. **b.** The flow chart of PT-PINNs. **c.** The network structure and the training process of PT-PINNs.

the residual loss is minimal, and effectively prevents oscillations in residuals caused by excessive fluctuations of turbulent viscosity during training. This method also allows us to directly initialize turbulent viscosity in the pre-training stage.

In this study, the effectiveness of the proposed framework is validated using a three-dimensional parameterized turbulent backward-facing step (BFS) flow problem. The validation is performed using parameterized experiments conducted by Nadge et al. [33], with Reynolds numbers $Re_h = 6000$ – 67000 , step expansion ratios $ER=1.1, 1.3, 1.5, 1.84$, and 2.50 . As shown in Fig. 1a, The trained parameterized step flow prediction model includes two variable parameters: the geometric parameter step expansion ratio (ER) and the step Reynolds number (Re_h). The step expansion ratio $ER = (H + h)/H$ is controlled by varying the step height $h \in [0.4, 2]$ m while keeping the inlet height $H = 4$ m fixed. The Reynolds number $Re_h = Uh/\nu$

is controlled by varying the step height and fluid viscosity $\nu \in [0.00003, 0.0004]$ m²/s while keeping the inlet velocity $U = (3, 0, 0)$ m/s fixed. The specific geometric proportions of the problem are consistent with the experiments, with the specific dimensions being $S = 24$ m, $L = 52$ m, and $L_2 = 40$ m. The Reynolds number for the trained parameterized step flow prediction model ranges from $Re_h \in [3000, 20,000]$, and the step expansion ratio ranges from $ER \in [1.1, 1.5]$. In this study, the symbol Re represents Re_h .

The $k-\omega$ turbulence model [34] was employed to solve the parameterized turbulence problem. The Launder-Spalding wall function [35] was applied as wall boundary conditions and a velocity correction function was incorporated into the bottom wall boundary condition. No additional data were introduced in the flow field to assist the training. In addition to experimental results, we also compared the model predictions with computational fluid dynamics (CFD) results. The CFD results were obtained

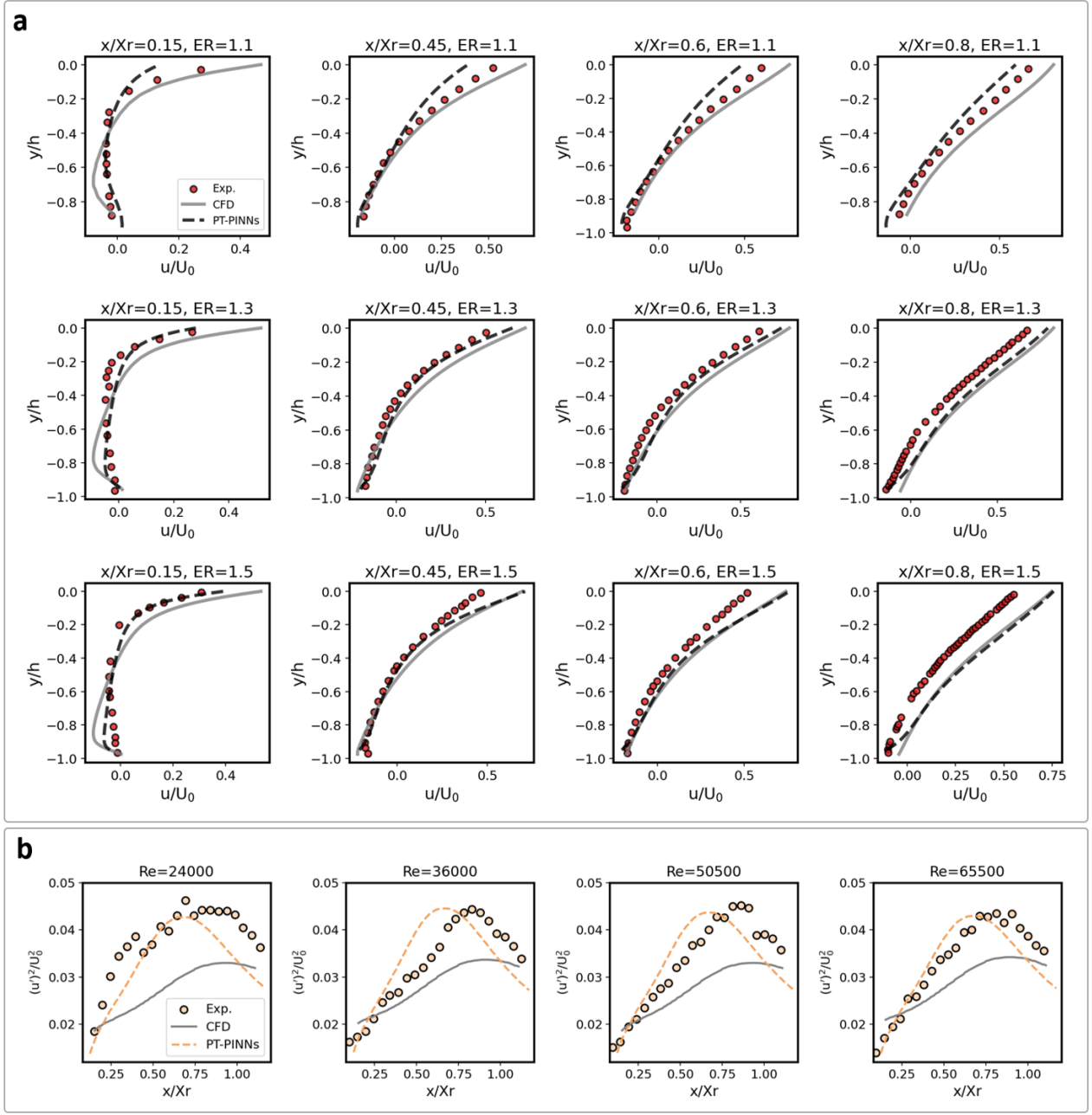


FIG. 2. Quantitative comparisons of PT-PINNs' flow field velocity u and turbulence stress $(u')^2/U_0^2$ prediction with experimental [33] and CFD results in the recirculation region. **a.** Velocity u distribution of the section line at $x/Xr=0.15, 0.45, 0.6, 0.85$ positions in $Z=0$ Plane. **b.** Stream-wise variation of maximum turbulent stress $(u')^2/U_0^2$ under different Reynolds numbers when $ER=1.3$. The X axis is normalized by mean reattachment length Xr .

by simulating the step flow field for each corresponding condition using the finite volume method in the Fluent software [36]. The detailed settings for PINNs and CFD simulations will be explained in the Methods section.

Validation against Experiments and CFD Results

Fig. 2a presents a comparison of the stream-wise velocity u along various sectional lines within the recirculation region, as predicted by PT-PINNs, with experimental [33] and CFD results under different operating conditions. For the overall trend of velocity u variation along the sectional lines, PT-PINNs predictions achieve

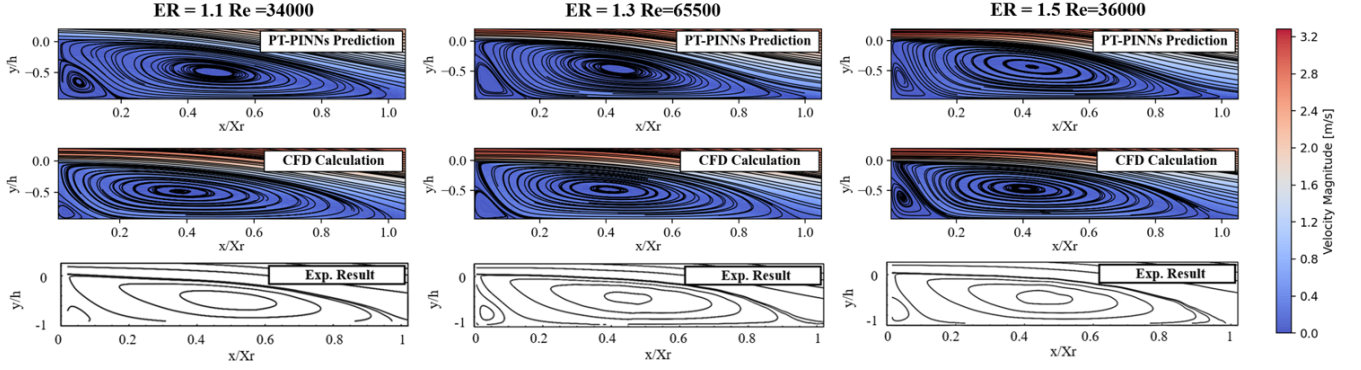


FIG. 3. Comparisons of PT-PINNs predictions of streamlines of the recirculation vortex at the $Z=0$ Plane with experimental [33] and CFD results under different Reynolds numbers and expansion ratios.

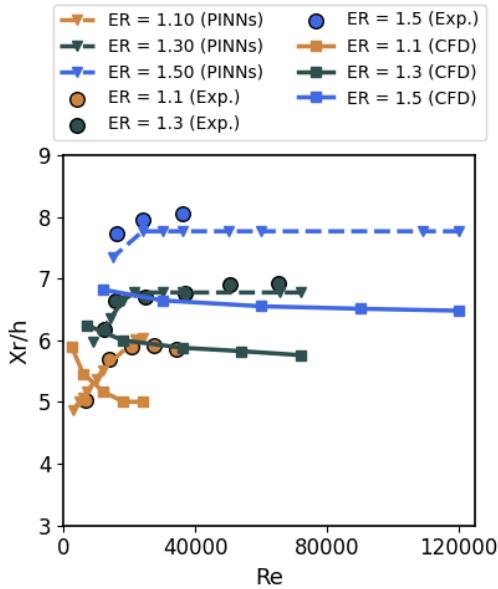


FIG. 4. Comparison of PT-PINNs' reattachment length predictions with CFD and experimental results [33].

good agreements with both CFD and experimental results. Moreover, the predictions of PT-PINNs at the section lines of $x/X_r = 0.15$ and 0.45 exhibit even better alignment with experimental measurements than CFD results under various conditions. This demonstrates that PT-PINNs can provide predictions of recirculation vortex structures that align more closely with experimental results under varying operating conditions. Furthermore, it illustrates that PINNs are not inherently incapable of accurately predicting flow field details. By guiding PINNs to correctly learn the governing partial differential equations and boundary conditions through appropriate network architectures and training strategies, PINNs can achieve parameterized three-dimensional turbulent flow field predictions that meet industrial accuracy require-

ments. Fig. 2b presents a comparison of the maximum turbulent stress $(u')^2/U_0^2$ across vertical cross-sections at different x position within the recirculation region, as predicted by PT-PINNs, with CFD and experimental results. Surprisingly, PT-PINNs achieve superior consistency with experimental data in terms of both the peak values and the overall distribution of maximum turbulent stress compared to CFD. This can be attributed to the utilization of automatic differentiation [17] and the mesh-free calculation in PINNs, which enables a more detailed traversal of the flow field space through a random point sampling strategy in each iteration, thereby reducing the numerical errors when solving PDEs.

Fig. 3 presents the comparisons of the flow field streamlines in the recirculation regions, as predicted by PT-PINNs, with experimental and CFD results across various step expansion ratios and Reynolds numbers. Without the aid of internal field data for training, PT-PINNs accurately predicted the shapes of both the corner vortex and the recirculation vortex, demonstrating consistency across different expansion ratios and Reynolds numbers with experimental results and reflecting the self-similarity characteristics of turbulence. Furthermore, as illustrated in Fig. 4, due to the application of refined boundary conditions based on experimental results, PT-PINNs can predict the reattachment length variation concerning the expansion ratio and Reynolds number more accurately, aligning more closely with experimental measurements than traditional CFD methods. At high Reynolds numbers, the prediction of the reattachment length by CFD significantly deviates from the actual experimental measurements. This implies that while CFD can predict the overall shape of the recirculation vortex, the predicted vortex size differs considerably from experimental results. In contrast, the predictions of PT-PINNs show a high degree of agreement with the experimental results. This demonstrates the potential of PINNs as a parametric solver for achieving higher prediction accuracy in engineering turbulence problems compared to traditional CFD methods. Although we implemented a smooth transition in the loss function weights for the wall

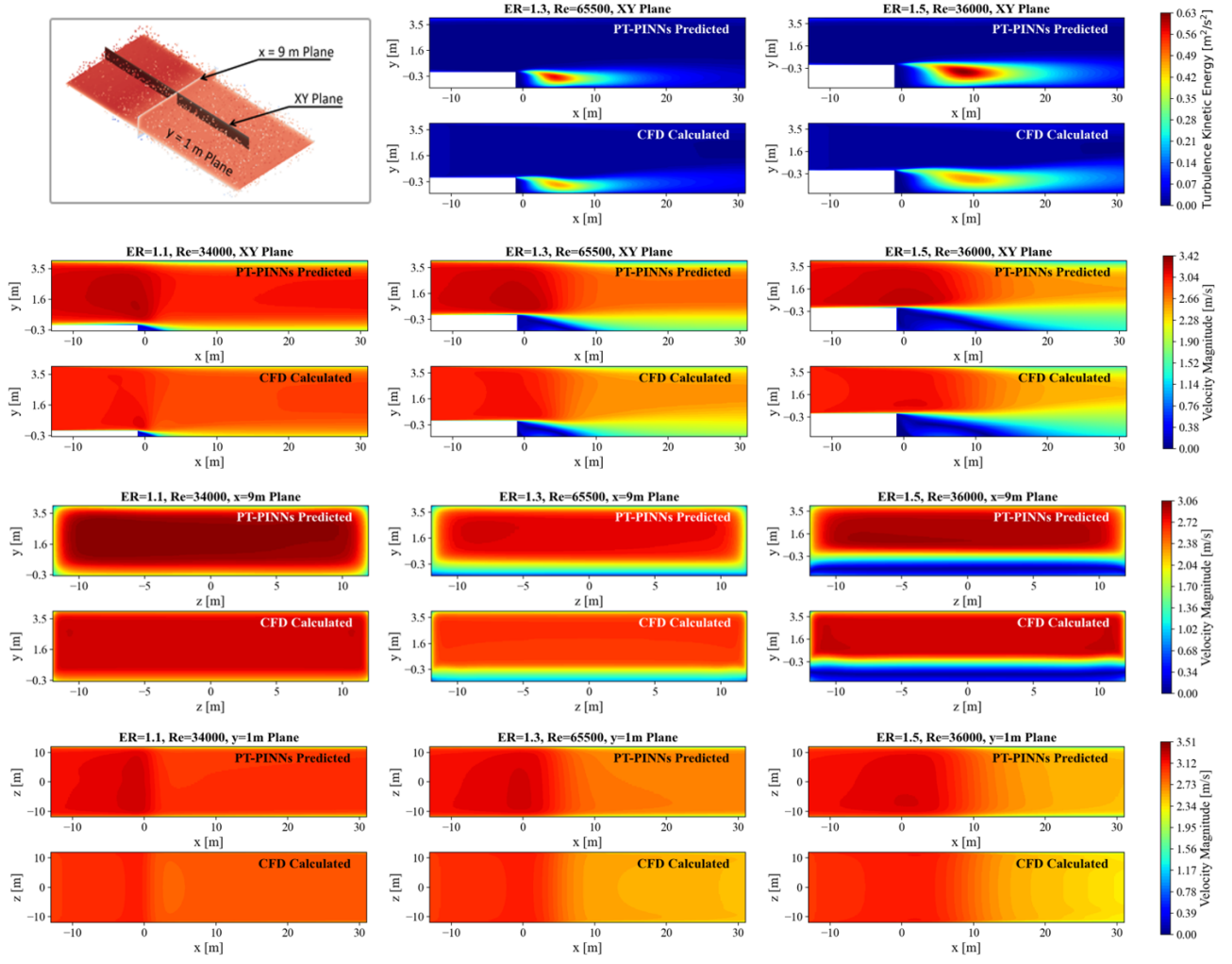


FIG. 5. Comparisons of PT-PINNs predictions against CFD results of overall flow fields.

functions at the intersection of the horizontal and vertical walls of the step, minor discrepancies in PT-PINNs' flow field predictions persist near the upper horizontal wall of the step. These discrepancies can be attributed to conflicting velocity predictions from the wall functions of the two intersecting walls.

Fig. 5 presents the comparisons of the overall flow field predictions for the three-dimensional step flow by PT-PINNs and CFD methods under various conditions. On the $z = 0$ m, $y = 1$ m, and $x = 9$ m plane the velocity predictions of PT-PINNs exhibit high consistency with the CFD results, with average relative errors in velocity magnitude of 5%, 6%, and 3%, respectively. In terms of turbulence parameters, the turbulence kinetic energy predicted by PINNs, which are generated by the velocity gradient variations, also shows good agreement with the CFD results. Due to the application of the refined boundary condition based on experiment results [33, 39] at the bottom wall and the mesh-free nature of PINNs, the turbulence kinetic energy generated near the step is significantly higher than the CFD results but achieves

better consistency with experimental results, as validated in Fig. 2b.

Table I presents the comparisons of the settings, solution time, and model size between PT-PINNs and the CFD methods for solving parameterized backward step flow. Traditional CFD methods require multiple simulations to obtain the parameterized flow field distributions. If a lightweight parameterized prediction model is needed, training based on these simulation data is also required. PT-PINNs, however, directly generate a lightweight neural network model capable of predicting parameterized turbulent proxy flow fields through a single training process, without the need for multiple simulations. Moreover, the model size is only 1% of a single CFD case. For the three-dimensional parameterized step flow case in this section, in terms of parameterized model construction time, the PT-PINNs method achieves an acceleration factor of 16 compared to CFD with multiple simulations (using a full-factorial parameter value design for 21×21 simulations). Regarding the obtaining of flow fields with the same resolution for a single operating con-

TABLE I. Comparisons of PT-PINNs and the CFD method.

PT-PINNs training based on Nvidia Modulus platform [37]								
Inputs	Outputs	Hidden layers \times neurons	Interior batchsize	Epoches	Time costs (h)	Inference speed speed (s)	GPU device	Model Size (MB)
x, y, z, ν , ER	u, v, w, p, k, ω	7×512	2048	400000	39	40	1 \times RTX4090 GPU	12.1
CFD method based on ANSYS-Fluent software [38]								
Inputs	Outputs	Finite cells	Simulation iterations	Case number	Time costs (h)	Time costs per case (h)	CPU device	Data size per case (GB)
x, y, z	u, v, w, p, k, ω	8000000	400	21^2	632	1.5	1 \times AMD EPYC 7b12	1.07

Note: The values of finite cells and Time costs per case are average values. The CPU and GPU devices are of equivalent procurement cost. The CPU device has 64 cores and is paired with 128 GB of memory.

dition, the inference time of PT-PINNs is also only 1% of that of a single CFD simulation. This indicates that PT-PINNs hold promising prospects as a solver for parameterized engineering turbulent flow problems.

Turbulent Viscosity Constraint and Flow Fields Initialization

We developed two methods to enhance the PT-PINNs' ability to solve parameterized turbulent flow fields. The first method involves taking turbulent viscosity as a network output and transforming its algebraic expression into a soft constraint within the network architecture and training process. The second method is a pre-training method based on parameterized boundary conditions and flow field mass conservation. Fig. 6 demonstrates the effects of these methods on PT-PINNs' parameterized turbulent flow field solving. During the training process, we designed three distinct PDEs weight balancing schemes to further investigate the roles of these methods in avoiding local optima and reducing the sensitivity of model training to loss balancing. The three PDEs weight balancing schemes, corresponding to well-balanced weights, poorly balanced weights, and excessively imbalanced weights, are defined by the weight ratios of continuity-equation: momentum-equations: k-equation: ω^+ -equation as 1:10:0.1:1, 1:10:10:100, and 1:10:100:1000, respectively. When the weights balance is well balanced and pre-training is applied, both neural networks with and without ν_t output achieve accurate overall flow field predictions (Fig. 6a and Fig. 6d). The relative errors of the velocity u compared to CFD results (Fig. 6h) were 7.5% and 7.6%, respectively. However, under poorly balanced PDEs weights during training, the network without ν_t output produced significantly degraded predictions (Fig. 6e), with the u-velocity field error reaching 14.9%, compared to 9.4% for PT-PINNs with ν_t output trained under the same weights. Furthermore, the turbulent kinetic energy distribution near separation vortexes deviated significantly, resembling the trend observed in Fig. 6g for the network trapped in a local optimum. Additionally, if the network with ν_t output is trained under a well-balanced weight but without

pre-training applied, similar issues of the turbulent kinetic energy distribution arise. Its relative error of the velocity u increases to 10.5%, whereas the error for the viscosity-output network without initialization remains low at 7.8%. Fig. 6g illustrates the results of a network trapped in a local optimum due to imbalanced weight training. In this local optimum, the network sets turbulent kinetic energy to zero in regions where it should be high, achieving a physically unrealistic loss minimization. When the weight balance is poorly balanced and pre-training is not applied or the weight balance is excessively imbalanced, the PT-PINNs' predictions exhibit the same issues.

Fig. 7 illustrates the evolution of the total loss during training using different methods. PT-PINNs exhibit better convergence under both well-balanced and poorly balanced weights. However, PT-PINNs without the turbulent viscosity output method exhibit significantly greater oscillations during training with poorly balanced weights. Fig. 7c compares the loss curves of PT-PINNs trained with and without pre-training method. The former achieves faster and more robust convergence, requiring only 20,000 iterations without differential equation constraints (approximately 40 minutes), whereas the latter converges slowly. Fig. 7d compares the iterative processes of networks trapped in local optima with those of a well-trained network. Networks trapped in local optima exhibit significantly higher converged losses compared to those avoiding local optima, though still within a relatively small range relative to the initial loss.

DISCUSSION

The parameterized prediction of turbulent flows is of significant importance in various engineering designs and digital twin scenarios. As a new partial differential equation solver leveraging neural networks, PINNs exhibit inherent advantages in addressing parameterized high-dimensional problems. In this study, we proposed a PINNs-based framework for solving parameterized steady-state turbulent problems, PT-PINNs. By incorporating turbulent viscosity as a network output and employing a flow-field-based pre-training method,

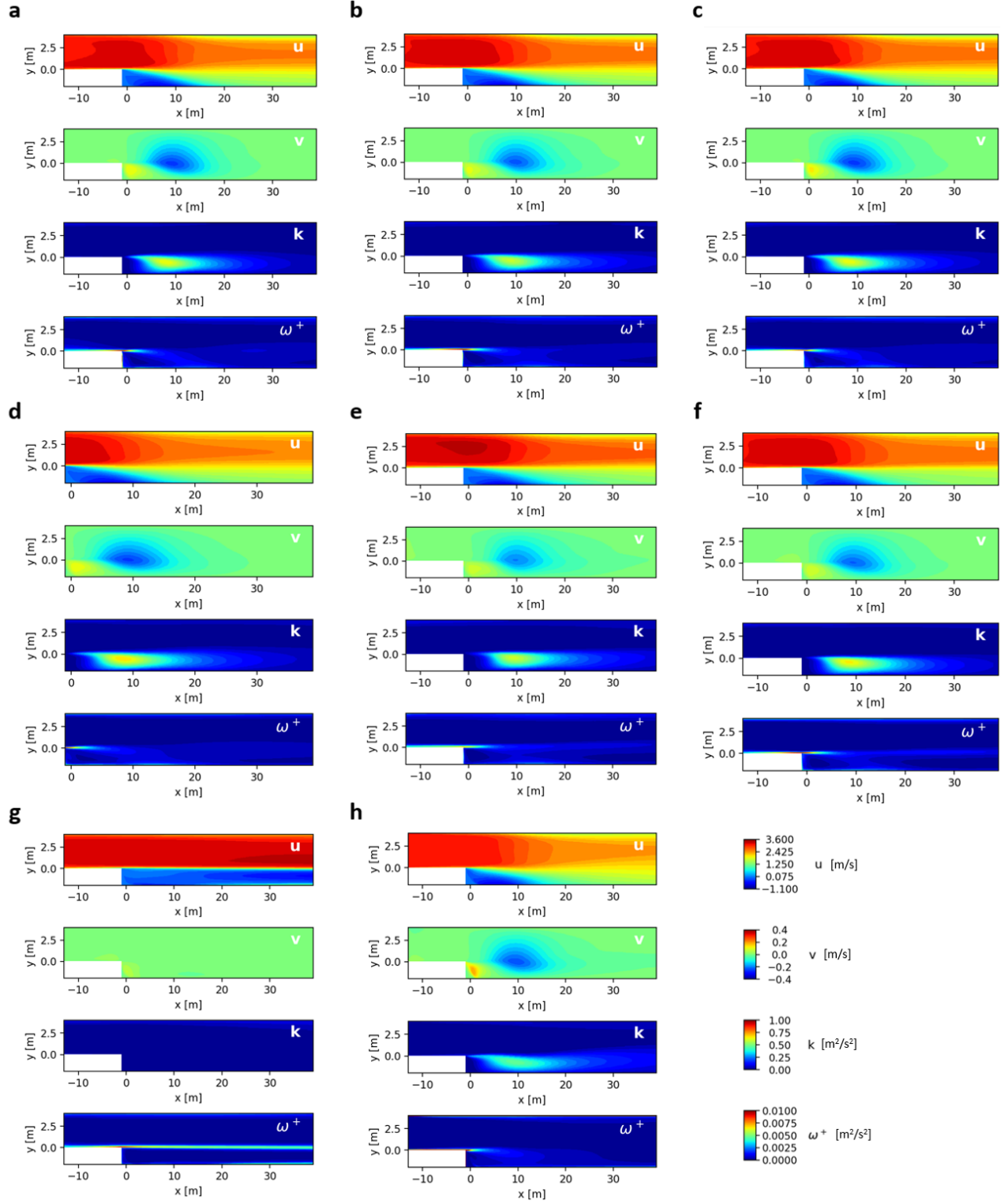


FIG. 6. Comparisons of flow fields of $ER = 1.5, Re = 30000$ predicted by different networks under different weights balancing and pre-training methods. **a.** The prediction of PT-PINNs trained with ν_t output network and pre-training under well-balanced weights. **b.** The prediction of PT-PINNs trained with ν_t output network and pre-training under poorly balanced weights. **c.** The prediction of PT-PINNs trained without using the pre-training method under well-balanced weights. **d.** The prediction of PT-PINNs trained without ν_t output network under well-balanced weights. **e.** The prediction of PT-PINNs trained without ν_t output network under poorly balanced weights. **f.** The prediction of PT-PINNs trained without ν_t output network or pre-training under well-balanced weights. **g.** The prediction of PT-PINNs trained without ν_t output network or pre-training under poorly balanced weights. **h.** CFD results.

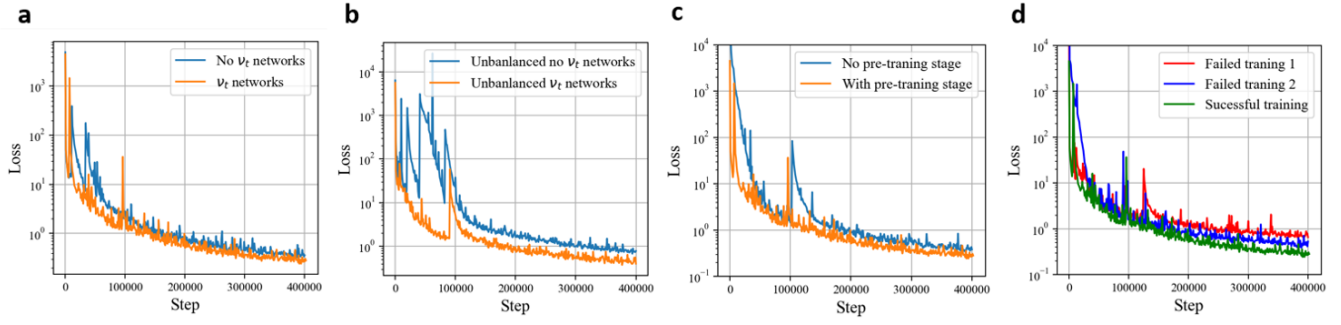


FIG. 7. **Comparisons of loss curves for different networks under different weights balancing and pre-training methods.** **a.** PT-PINNs with and without ν_t output network, trained with well-balanced weights. **b.** PT-PINNs with and without ν_t output network, trained with poorly balanced weights. **c.** PT-PINNs trained with and without the pre-training method under well-balanced weights. **d.** PT-PINNs with ν_t output network and pre-training method trained under well-balanced weights compared to PT-PINNs without the pre-training method, trained under poorly balanced weights (failed training 1), and PT-PINNs without ν_t output network, trained under poorly balanced weights (failed training 2).

we successfully enhance the prediction capability of PT-PINNs for engineering turbulence problems.

Using PT-PINNs, this study solved a parameterized three-dimensional backward-facing step flow problem based on the $k-\omega$ turbulence model without using any interior flow data for training. We obtained a model that can quickly predict the parametric flow fields using only one training process by PT-PINNs. The model includes two variable parameters, fluid viscosity, and step height, and can perform predictions for three-dimensional backward-facing step flows under arbitrary conditions with $Re=3000-200,000$ and $ER=1.1-1.5$. The model's prediction capability was validated by comparing its results against Nadge's experimental data [33] and CFD results. The model demonstrates good agreement with CFD simulation results in terms of the overall flow field, with relative velocity field errors kept below 6%. For detailed comparisons in the recirculation regions, the shapes of the primary recirculation and corner vortexes closely match the experimental results. In some cases, the model's stream-wise velocity and turbulence stress predictions are even closer to experimental results than CFD simulations.

Regarding computational efficiency, training the model using the PT-PINNs framework took approximately 39 hours. While this duration is longer than a single CFD simulation, parameterized problems generally require hundreds or even thousands of CFD simulations. For instance, the PT-PINNs method achieves an acceleration factor of 16 compared to running multiple CFD simulations (using a full-factorial parameter design for 21×21 simulations). Furthermore, once trained, PT-PINNs can infer flow fields for any operating condition with an equivalent mesh resolution in just 40 seconds—only 1% of the time required for a single CFD simulation.

Additionally, we validated the superiority of the two methods applied in the PT-PINNs framework for steady-

state turbulent problems by solving the backward-facing step flow using the $k-\omega$ models with different methods. Comparisons of different training methods show that the pre-training method and the method of treating turbulent viscosity as a network output help PT-PINNs maintain accurate predictions of turbulent flows, even under poorly balanced training weights. In contrast, PT-PINNs without these two methods often produce poor predictions under various conditions and are more prone to converging to completely non-physical local optima.

METHODS

Turbulence Modeling

This work focuses on the steady-state incompressible Reynolds-averaged turbulence. The standard $k-\omega$ model [34] is employed to solve the parametrized three-dimensional turbulent backward-facing step flow problem in this study. The specific governing equations are as follows:

$$\frac{\partial u_i}{\partial x_i} = 0 \quad (1)$$

$$u_j \frac{\partial u_i}{\partial x_j} + \frac{1}{\rho} \frac{\partial p}{\partial x_i} - \frac{\partial}{\partial x_j} \left[(\nu + \nu_t) \frac{\partial u_i}{\partial x_j} \right] = 0 \quad (2)$$

$$u_j \frac{\partial k}{\partial x_j} = \frac{\partial}{\partial x_j} \left[\left(\nu + \frac{\nu_t}{\sigma_k} \right) \frac{\partial k}{\partial x_j} \right] + \frac{1}{\rho} (P_k - Y_k) \quad (3)$$

$$u_i \cdot \frac{\partial \omega}{\partial x_i} = \frac{\partial}{\partial x_j} \left[\left(\nu + \frac{\nu_t}{\sigma_\omega} \right) \frac{\partial \omega}{\partial x_j} \right] - \frac{1}{\rho} (P_\omega - Y_\omega) \quad (4)$$

where u_i and p are the Reynolds-averaged flow velocity and pressure, the density $\rho = 1 \text{ kg/m}^3$ is constant.

$\sigma_k = \sigma_\omega = 2$ are model constants. $P_k = \rho \nu_t G$ represents the turbulent kinetic energy generation term. \sqrt{G} represents the average strain rate tensor, and $G = 2(u_x^2 + v_y^2 + w_z^2) + (u_y + v_x)^2 + (u_z + w_x)^2 + (v_z + w_y)^2$. $Y_k = \rho \beta^* k \omega$ represents the turbulent kinetic energy dissipation term, where $\beta^* = 0.09$. $P_\omega = \rho \alpha G$ represents the turbulent specific dissipation rate generation term, where $\alpha = 5/9$. $Y_\omega = \rho \beta \omega^2$ represents the turbulent dissipation rate dissipation term, where $\beta = 0.075$. The eddy viscosity ν_t is closed using the k- ω turbulence model, which is given by the following formula:

$$\nu_t = \frac{k}{\omega} \quad (5)$$

Lauder-Spalding wall functions [35] are utilized to solve the near wall flow. The relations for Launder-Spalding wall functions formulation are similar to standard wall functions, except now the friction velocity can directly be computed from the turbulent kinetic energy as shown below:

$$u_\tau = C_\mu^{1/4} k^{1/2} \quad (6)$$

$$y^+ = \frac{\rho u_\tau y_p}{\mu} \quad (7)$$

$$U = \frac{C_\mu^{1/4} k^{1/2}}{\kappa} \ln(Ey^+) \quad (8)$$

$$\omega = (1 - F) \frac{u_\tau}{0.3\kappa y} + F \frac{6\nu}{0.075y^2} \quad (9)$$

$$\tau_w \equiv \mu \frac{\partial U}{\partial y} \Big|_w \approx (\mu + \mu_t) \frac{\partial U}{\partial y} \Big|_P = \frac{\rho C_\mu^{1/4} k^{1/2} U \kappa}{\ln(Ey^+)} \quad (10)$$

where u_τ is the friction velocity, U is the mean velocity at the near wall region, y^+ is the dimensionless distance from the wall, τ_w is the wall shear stress. y is the distance to the wall which is set as a constant in each wall constraint which is similar to y_p in CFD computations. In CFD computations, wall functions are applied to the first layer of grid cells near the wall. Therefore, the dimensionless parameter y^+ is calculated based on the height of the center of the first grid cell, y_p . The height y_p needs to be set by estimating the turbulent boundary layer height according to the flow conditions. The function F is introduced to smooth the ω calculations in different regions, which is defined as: $F = (\tanh(10 - y^+) + 1.0)^{0.5}$.

When using wall functions for turbulent flow simulations, the turbulent flow in the separation and recirculation regions often can not be accurately predicted. As shown in Fig. 4, the predicted reattachment length using the wall-function-based CFD method demonstrated poor agreement with experimental results across the parameter space. Based on the summaries of the wall shear stress and reattachment point distribution from Nade

et al. [33] and Jovic and Driver [39] for backward-facing step flows, a set of empirical formulas was employed to modify the wall functions velocity for the boundary conditions at the bottom and vertical walls:

$$v_{ve} = 0.07 \sin(2\pi y^2/h^2 - \pi) \quad (11)$$

$$u_{bo} = \begin{cases} 0.025 \cdot (\operatorname{erf}(16(0.5 + (x - 0.6h)/h)) \\ + \operatorname{erf}(16(0.5 - (x - 0.6h)/h))), \\ \quad \text{if } 0 \leq x < 1.2h, \\ 0.65 \cdot \sin(\pi(x - X_r)/(X_r - h)), \\ \quad \text{if } 1.5h \leq x < X_r + 1.2h, \\ 1.76ER \quad \text{if } X_r + 8h \leq x, \end{cases} \quad (12)$$

$$X_r = c_{re} \cdot (4.95 * ER + 0.5) \cdot h \quad (13)$$

$$c_{re} = \operatorname{Min}(1, 1 - 0.000011 * (20000 - Re_h)) \quad (14)$$

where x and y are the horizontal and vertical distance to the downstream step corner, and X_r is the reattachment length. v_{ve} is the wall boundary velocity of the vertical wall, u_{bo} is the wall boundary velocity of the bottom wall.

Physics Informed Neural Networks

This work employs the Physics-Informed Neural Networks (PINNs) method as a parameterized solver to address the parameterized flow problem. Its input X includes spatial coordinates as well as arbitrary geometric, operating conditions, and physical property parameters relevant to the problem. The output Y represents the flow field variables, and the relationship between them is established through a fully connected neural network, which can be mathematically expressed as follows:

$$H_1 = \sigma(w_1 X + b_1) \quad (15)$$

$$H_l = \sigma(W_{l-1} H_{l-1} + b_l) \\ \text{for } l = 2, 3, \dots, n \quad (16)$$

$$Y(X) = W_{n+1} H_n + b_{n+1} \quad (17)$$

where, W and b are the network weights and biases, n is the number of hidden layers, and σ is the activation function. The input X is mapped through the network with multiple hidden layers H_l , deriving the relationship between the variables in Y and the parameters in X . During the iterative process, automatic differentiation is used [17] to calculate the derivatives of the output Y with respect to X , enabling the solution of differential equations in the physics loss function. The iterative correction of weights and biases can be viewed as fitting a specific function that complies with physical constraints in the

parameterized space. In this work, the loss functions are expressed as:

$$L_{\text{total}} = L_{\text{PDE}} + L_{\text{BC}} \quad (18)$$

$$L_{\text{PDE}} = w_1 L_{\text{continuity}} + w_2 L_{\text{momentum}} + w_3 L_{k-\text{transpot}} + w_4 L_{\omega-\text{transpot}} \quad (19)$$

$$L_{\text{BC}} = w_5 L_{\text{inlet}} + w_6 L_{\text{outlet}} + w_7 L_{\text{wall-function}} \quad (20)$$

$$L_{\nu_t} = w_8 ||(\nu_t \omega - k)||^2 + w_9 ||(\nu_t - \frac{k}{\omega})||^2 \quad (21)$$

where w_i represents the weights of each residual in the loss functions. The turbulence viscosity constraint starts with a weaker constraint in the initial steps and transitions to a stronger one later. The transfer is defined as follow:

$$w_8 = (\tanh((120000 - n_{\text{step}}) \times 5 \times 10^{-5}) + 1) \times 0.5 \quad (22)$$

$$w_9 = 1 - w_8 \quad (23)$$

where n_{step} is the iteration step number during training. Since the presence of ω in the denominator in the constraint of $\nu_t = \frac{k}{\omega}$ often causes significant oscillations in the loss function during training, this strategy enables the neural network to first learn the overall flow field by initially incorporating a weaker form of the constraint, then progressively refining the detailed flow field through a gradual transition to the stronger form.

In this study, most other weights of loss functions are specified constant values. At the step's vertical wall, we

applied a smooth weight transition to minimize the influence of corner points on training:

$$w_{\text{normal-vel}} = (\text{erf}(64 \cdot (0.5 + (y + h/2)/0.9h))) + \text{erf}(64 \cdot (0.5 - (y + h/2)/0.9h)) \quad (24)$$

A pre-training step is introduced as flow field initialization before formal training. In this step, the governing partial differential equation constraints are not applied to the interior field. For the velocity field, specific regions are directly constrained using constant values based on mass conservation, while other regions used integrated interfaces to maintain mass conservation. Boundary conditions are applied normally in the pre-training stage. For other physical quantities, constant values are directly assigned. For the BFS flow case in this study, the loss functions of pre-training stage can be expressed as:

$$L_{\text{init}} = w_{10} L_{\text{interior-1, init-u}} + w_{11} L_{\text{interior-2, init-u}} + w_{12} L_{\text{interior, init-v}} + w_{13} L_{\text{interior, init-w}} + w_{14} L_{\text{wall-function}} + w_{15} L_{\text{interior, init-}\nu_t} \quad (25)$$

$$L_{\text{interior-1, init-u}} = u - u_{\text{inlet}} \quad (26)$$

$$L_{\text{interior-2, init-u}} = u - u_{\text{inlet}}/ER \quad (27)$$

$$L_{\text{interior, init-v}} = v \quad (28)$$

$$L_{\text{interior, init-w}} = w \quad (29)$$

$$L_{\text{interior, init-}\nu_t} = \nu_t - 0.003 \quad (30)$$

where interior-1 represents the fluid region upstream of the step, while interior-2 denotes the fluid region located $x > 10h$ downstream of the step corner. To ensure flow rate conservation within the fluid region between these two areas, we apply several integral sections.

The Adaptive Moment Estimation (Adam) optimizer [40] was used to adjust the parameters of the neural network model. The initial learning rate is set to 0.0001, and it decays to 95% of its original value every 8,000 steps. The training is repeated iteratively until the loss function reaches the user-defined threshold.

-
- [1] P. Schmitt, T. Poinot, B. Schuermans, and K. P. Geigle, Large-eddy simulation and experimental study of heat transfer, nitric oxide emissions and combustion instability in a swirled turbulent high-pressure burner, *Journal of Fluid Mechanics* **570**, 17–46 (2007).
 - [2] Z. Lyu and J. R. R. A. Martins, Aerodynamic design optimization studies of a blended-wing-body aircraft, *Journal of Aircraft* **51**, 1604 (2014), 43rd AIAA Fluid Dynamics Conference and Exhibit, San Diego, CA, JUN 24-27, 2013.

- [3] A. H. Khalaj and S. K. Halgamuge, A review on efficient thermal management of air- and liquid-cooled data centers: From chip to the cooling system, *Applied Energy* **205**, 1165 (2017).
- [4] M. Mohan Rai and P. Moin, Direct simulations of turbulent flow using finite-difference schemes, *Journal of Computational Physics* **96**, 15 (1991).
- [5] C. RHIE and W. CHOW, Numerical study of the turbulent-flow past an airfoil with trailing edge separation, *AIAA Journal* **21**, 1525 (1983).

- [6] F. Bassi, A. Crivellini, S. Rebay, and M. Savini, Discontinuous galerkin solution of the reynolds-averaged navier-stokes and k-omega turbulence model equations, *Computers & Fluids* **34**, 507 (2005), workshop on Residual Distribution Schemes, Discontinuous Galerkin Schemes, Multidimensional Schemes and Mesh Adaptation, Univ Bordeaux I, Inst Math, Talence, France, JUN 23-25, 2002.
- [7] S. A. Orszag and A. T. Patera, Secondary instability of wall-bounded shear flows, *Journal of Fluid Mechanics* **128**, 347–385 (1983).
- [8] S. Chikatamarla, C. Frouzakis, I. Karlin, A. Tomboulides, and K. Boulouchos, Lattice boltzmann method for direct numerical simulation of turbulent flows, *Journal of Fluid Mechanics* **656**, 298 (2010).
- [9] H. Pitsch, Large-eddy simulation of turbulent combustion, *Annual Review of Fluid Mechanics Annual Review of Fluid Mechanics*, **38**, 453 (2006).
- [10] P. Spalart, Strategies for turbulence modelling and simulations, *International Journal of Heat and Fluid Flow* **21**, 252 (2000), 4th International Symposium on Engineering Turbulence Modelling and Measurements, AJACCIO, France, MAY, 1999.
- [11] X. Guo, W. Li, and F. Iorio, Convolutional neural networks for steady flow approximation, in *KDD '16: Proceedings of the 22nd ACM SIGKDD International Conference on Knowledge Discovery and Data Mining* (Assoc Comp Machinery; Assoc Comp Machinery SIGMOD; Assoc Comp Machinery SIGKDD, 2016) pp. 481–490, 22nd ACM SIGKDD International Conference on Knowledge Discovery and Data Mining (KDD), San Francisco, CA, AUG 13-17, 2016.
- [12] H. F. S. Lui and W. R. Wolf, Construction of reduced-order models for fluid flows using deep feedforward neural networks, *Journal Of Fluid Mechanics* **872**, 963 (2019).
- [13] T. Nakamura, K. Fukami, K. Hasegawa, Y. Nabae, and K. Fukagata, Convolutional neural network and long short-term memory based reduced order surrogate for minimal turbulent channel flow, *Physics of Fluids* **33**, 10.1063/5.0039845 (2021).
- [14] L. Lu, P. Jin, and G. E. Karniadakis, Deeponet: Learning nonlinear operators for identifying differential equations based on the universal approximation theorem of operators, *arXiv preprint arXiv:1910.03193* (2019).
- [15] Z. Li, N. Kovachki, K. Azizzadenesheli, B. Liu, K. Bhattacharya, A. Stuart, and A. Anandkumar, Fourier neural operator for parametric partial differential equations, *arXiv preprint arXiv:2010.08895* (2020).
- [16] M. Raissi, P. Perdikaris, and G. E. Karniadakis, Physics-informed neural networks: A deep learning framework for solving forward and inverse problems involving nonlinear partial differential equations, *Journal of Computational physics* **378**, 686 (2019).
- [17] A. G. Baydin, B. A. Pearlmutter, A. A. Radul, and J. M. Siskind, Automatic differentiation in machine learning: a survey, *Journal of Machine Learning Research* **18**, 1 (2018).
- [18] Y. Sun, U. Sengupta, and M. Juniper, Physics-informed deep learning for simultaneous surrogate modeling and pde-constrained optimization of an airfoil geometry, *Computer Methods in Applied Mechanics and Engineering* **411**, 116042 (2023).
- [19] X. Jin, S. Cai, H. Li, and G. E. Karniadakis, Nsfnets (navier-stokes flow nets): Physics-informed neural networks for the incompressible navier-stokes equations, *Journal of Computational Physics* **426**, 109951 (2021).
- [20] F. Pioch, J. H. Harmening, A. M. Müller, F.-J. Peitzmann, D. Schramm, and O. el Moctar, Turbulence modeling for physics-informed neural networks: Comparison of different rans models for the backward-facing step flow, *Fluids* **8**, 10.3390/fluids8020043 (2023).
- [21] V. Yadav, M. Casel, and A. Ghani, Rf-pinns: Reactive flow physics-informed neural networks for field reconstruction of laminar and turbulent flames using sparse data, *Journal of Computational Physics*, 113698 (2024).
- [22] S. Cai, Z. Mao, Z. Wang, M. Yin, and G. E. Karniadakis, Physics-informed neural networks (pinns) for fluid mechanics: A review, *Acta Mechanica Sinica* **37**, 1727 (2021).
- [23] S. Ghosh, A. Chakraborty, G. O. Brikis, and B. Dey, Using parametric pinns for predicting internal and external turbulent flows (2024), *arXiv:2410.18917* [cs.LG].
- [24] Z. Cao, K. Liu, K. Luo, Y. Cheng, and J. Fan, Efficient optimization design of flue deflectors through parametric surrogate modeling with physics-informed neural networks, *Physics of Fluids* **35** (2023).
- [25] A. Gafoor CTP, S. Kumar Boya, R. Jinka, A. Gupta, A. Tyagi, S. Sarkar, and D. N. Subramani, A physics-informed neural network for turbulent wake simulations behind wind turbines, *Physics of Fluids* **37** (2025).
- [26] W. Cao, X. Shan, S. Tang, W. Ouyang, and W. Zhang, Solving parametric high-reynolds-number wall-bounded turbulence around airfoils governed by reynolds-averaged navier-stokes equations using time-stepping-oriented neural network, *Physics of Fluids* **37**, 015151 (2025).
- [27] W. Cao and W. Zhang, Tsomn: Time-stepping-oriented neural network for solving partial differential equations (2023), *arXiv:2310.16491* [cs.LG].
- [28] B. Moseley, A. Markham, and T. Nissen-Meyer, Finite basis physics-informed neural networks (fbpinns): a scalable domain decomposition approach for solving differential equations, *Advances in Computational Mathematics* **49**, 10.1007/s10444-023-10065-9 (2023).
- [29] Z. Li, H. Zheng, N. Kovachki, D. Jin, H. Chen, B. Liu, K. Azizzadenesheli, and A. Anandkumar, Physics-informed neural operator for learning partial differential equations (2023), *arXiv:2111.03794* [cs.LG].
- [30] K. Liu, K. Luo, Y. Cheng, A. Liu, H. Li, J. Fan, and S. Balachandar, Parameterized physics-informed neural networks (p-pinns) solution of uniform flow over an arbitrarily spinning spherical particle, *International Journal of Multiphase Flow* **180**, 104937 (2024).
- [31] K. Liu, K. Luo, Y. Cheng, A. Liu, H. Li, J. Fan, and S. Balachandar, Surrogate modeling of parameterized multi-dimensional premixed combustion with physics-informed neural networks for rapid exploration of design space, *Combustion and Flame* **258**, 113094 (2023).
- [32] W. Cao, S. Tang, Q. Ma, W. Ouyang, and W. Zhang, Solving all laminar flows around airfoils all-at-once using a parametric neural network solver (2025), *arXiv:2501.01165* [physics.flu-dyn].
- [33] P. M. Nadge and R. Govardhan, High reynolds number flow over a backward-facing step: structure of the mean separation bubble, *Experiments in Fluids* **55**, 1 (2014).
- [34] D. C. Wilcox, Reassessment of the scale-determining equation for advanced turbulence models, *AIAA journal* **26**, 1299 (1988).

- [35] J. Bredberg, On the wall boundary condition for turbulence models, Chalmers University of Technology, Department of Thermo and Fluid Dynamics. Internal Report 00/4. Göteborg, 8 (2000).
- [36] FLUENTtheory, Ansys-fluent, Website (2024), https://ansyshelp.ansys.com/account/secured?returnurl=/Views/Secured/corp/v241/en/flu_th.html.
- [37] Modulus, Modulus, Website (2024), <https://catalog.ngc.nvidia.com/orgs/nvidia/teams/modulus/containers/modulus>.
- [38] ANSYS, Ansys-fluent, Website (2024), <https://www.ansys.com/products/fluids/ansys-fluent>.
- [39] S. Jović and D. M. Driver, Reynolds number effect on the skin friction in separated flows behind a backward-facing step, *Experiments in Fluids* **18**, 464 (1995).
- [40] D. P. Kingma and J. Ba, Adam: A method for stochastic optimization, arXiv preprint arXiv:1412.6980 (2014).

ACKNOWLEDGMENT

This work was supported in part by the National Natural Science Foundation of China under Grant 52236002

(K.L.(Kun Luo)).

AUTHOR CONTRIBUTIONS

L.J.(Liang Jiang) was responsible for conceptualization, methodology design, conducting numerical experiments, and drafting the original manuscript. Y.C.(Yuzhou Cheng) and K.L.(Kun Luo) extensively reviewed and edited the manuscript, providing valuable suggestions and revisions. Y.C. also contributed to methodology discussions. J.F.(Jianren Fan) and K.L. supervised the work

COMPETING INTERESTS

The authors declare no competing interests.